Accepted Manuscript

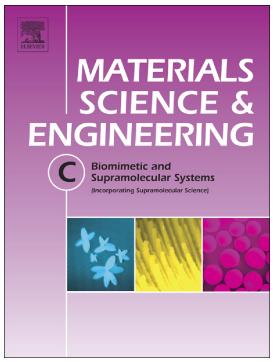

Composite material based on hydroxyapatite and multi-walled carbon nanotubes filled by iron: Preparation, properties and drug release ability

L.B. Sukhodub, L.F. Sukhodub, Yu.I. Prylutskyy, N.Yu. Strutynska, L.L. Vovchenko, V.M. Soroca, N.S. Slobodyanik, N.G. Tsierkezos, U. Ritter

PII: S0928-4931(18)30270-4
DOI: doi:10.1016/j.msec.2018.08.019
Reference: MSC 8813

To appear in: *Materials Science & Engineering C*

Received date: 26 January 2018
Revised date: 12 July 2018
Accepted date: 6 August 2018

Please cite this article as: L.B. Sukhodub, L.F. Sukhodub, Yu.I. Prylutskyy, N.Yu. Strutynska, L.L. Vovchenko, V.M. Soroca, N.S. Slobodyanik, N.G. Tsierkezos, U. Ritter , Composite material based on hydroxyapatite and multi-walled carbon nanotubes filled by iron: Preparation, properties and drug release ability. Msc (2018), doi:10.1016/j.msec.2018.08.019

Composite material based on hydroxyapatite and multi-walled carbon nanotubes filled by iron: preparation, properties and drug release ability

L.B. Sukhodub[1], L.F. Sukhodub[1], Yu.I. Prylutskyy[2], N.Yu. Strutynska[2], L.L. Vovchenko[2], V.M. Soroca[2], N.S. Slobodyanik[2], N.G. Tsierkezos[3], U. Ritter[3*]

[1]*Sumy State University, Sumy 40007, Ukraine*

[2]*Taras Shevchenko National University of Kyiv, Kyiv 01601, Ukraine*

[3]*Technical University of Ilmenau, Ilmenau 98693, Germany*

*Corresponding author: Uwe Ritter (E-mail: **uwe.ritter@tu-ilmenau.de**)

Abstract

The novel bioactive composite material based on hydroxyapatite and multi-walled carbon nanotubes filled by iron was synthesized by the "wet chemistry" method and characterized in detail by various experimental techniques including the X-ray diffraction, Fourier transform infrared and energy-dispersive X-ray fluorescence spectroscopy, thermogravimetric and differential thermal analysis. The swelling behaviour was quantified by measuring the changes in sample weight as a function of sample immersion time in a phosphate buffered saline (PBS). Bioactivity test was carried out by soaking the samples in PBS. The material composition influence on the model drug release was studied using the high-performance liquid chromatography method. Finally, the mechanical properties (maximal relative deformation, strength and Young's modulus) of the samples under loading were investigated too. The findings clear demonstrate the possibility of application of the created composite material in bioengineering of bone tissue to fill bone defects of various geometries with the function of prolonged release of the drug. It is assumed that this composite material can be used in 3D modeling of areas of bone tissue that have to bear a mechanical load.

Key words: hydroxyapatite, multi-walled carbon nanotubes filled by iron, drug release kinetics, bioactivity test, strength properties

1. Introduction

Nanocrystaline hydroxyapatite (HA) is widely used as an excellent material for the bone tissue engineering, in drug delivery systems, as biosensor and for many other applications due to chemical and biological similarity to the mineral part of bone [1,2]. HA is the most biocompatible orthophosphate among of all inorganic Ca/P materials. But it has many disadvantages namely negligible resorption rate, low mechanical strength and toughness, high shrinkage and deformation during sintering and, finally, unregulated biological properties. For these reasons in many cases HA is used in combination only with a biopolymer as a composite material.

Alginates are linear unbranched polysaccharides containing varying proportions of beta-D-mannuronate (M) and alpha-L-guluronate (G) residues. Sodium alginate (Alg) is very often used because of the low cost, biocompatibility, non-toxicity, chelating ability and of its potential use for the drug delivery systems [3-5]. Alg biopolymer carrying carboxylic group is able to form complexes with metal ions and is effective for the removal of heavy toxic metal cations [6]. Alg is a typical polyelectrolyte, it can be useful for sensing and modulating external chemical signals in the aqueous media [7]. The cross linking of Alg molecules with metal ions significantly reduced the Alg-based hydrogel swelling, and thus delayed the release of the entrapped drugs. As a result, Algs are being exploited in the controlled drug release systems [8-10].

Chlorhexidine (CH) is very common in medicine as an antibacterial agent against gram-positive and gram-negative bacteria and fungi [11]. The typical synthetic HA-based biocomposites include such biopolymers as collagen, chitosan, polylactide, cellulose, and many others bioactive substances [12], including the multi-walled carbon nanotubes (MWCNTs), as a promising candidate to prevent erosion of teeth [13]. The stimulus for the use in material science of CNTs, discovered in 1991 [14], is a set of their properties: remarkable mechanical and unique electrical properties, high thermal and chemical stability [15]. The excellent HA bioavailability

can be supplemented by the mechanical properties of CNTs in composite material. The formation of HA-based composites with CNTs content may logically lead to an expansion of the spectrum of properties without affecting biological activity, which is key to biomedical applications. The promise of CNT-Alg scaffolds in tissue engineering has been demonstrated in one of the first investigations of such composites [16], which has been confirmed in many further works [17,18]. CNTs have small dimensions, high strength and stiffness, high ratio of the length to diameter, that give them the excellent potential to use. MWCNTs consist of many graphene sheets, arranged concentrically. They have a diameter of 2 to 100 nm and a length from several micrometers to several millimeters. The chemistry of their surface allows them to be functionalized for specific applications [19]. MWCNTs are used in biosensors for determination of drugs and metal ions [20-35]. Since HA, as a chemical compound, is useful in the separation of proteins or nucleic acid by adsorption chromatography, the HA-based hybrid composites also can potentially be used in the field of sensory systems. Now MWCNTs are regarded as the most attractive functional excipients for nanomedicine [36,37], since they are capable to penetrate through a cellular plasma membrane [38], interact with DNA [39] can be tumor-targeted and have a central hollow core that can be loaded with a therapeutic drug [40]. The ability of MWCNTs to induce temperature increases compatible with thermal ablation and short near IR light exposure time suggests that these nanostructures may be useful as photothermal mediators [41]. At the same time, it should be noted, that CNTs can exhibit certain toxicity due to metallic impurities of catalytic action (iron, cobalt, nickel) [19], therefore it is necessary to pay attention to the biomaterials synthesis. On the other hand, the presence of CNTs in the biocomposite has no harmful side effects and could even enhance its bioactivity [42]. Finally, the modification of MWCNTs (intercalation and filling the internal cavities with different chemical elements) is a key tool to modulate their biodistribution and toxicity [43-45].

Hence, the aim of this research was to study the influence of MWCNTs filled by iron on the ability to adsorb and prolonged release of the drug and on the mechanical properties of the

formed composite biomaterial on the basis of HA, in order to use the material to create bone tissue model areas that are capable of bearing a mechanical load.

2. Materials and methods

2.1. *Materials*

The following materials and chemicals were used: MWCNTs filled by iron (MWCNT+Fe nanoparticles with a diameter 20-80 nm and a length up to 100 μm), prepared in accordance with [44, 46]. All structural parameters (SEM, TEM) together TG and XRD analysis of the used MWCNT are given previous and reported in [46]. The samples contain between 5 and 7 m% of iron. The main species are α-Fe together with small amounts of FeC and iron oxides. The clusters of iron or its compounds have an with average diameter of 10–15 nm and lengths of 120–140 nm.

Calcium nitrate tetrahydrate $Ca(NO_3)_2 \cdot 4H_2O$, diammonium dihydrophosphate ($(NH_4)_2HPO_4$), ammonium hydroxide NH_4OH, calcium chloride $CaCl_2$ (Sinopharm Chemical Reagent Co., Ltd), Alg ((low viscosity, E407, China), commercially available pharmaceutical CH (0.05%). All reagents were analytically grade and used as received.

2.2. *Composite material obtaining*

2.2.1. *HA suspensions*

At the first stage, HA suspension was obtained according to the "wet chemistry" method [47]. Briefly, for HA synthesis 50 ml of $Ca(NO_3)_2 \cdot 4H_2O$ (0.167 M) and 50 ml of $(NH_4)_2HPO_4$ (0.1 M) were used. Ammonium hydrophosphate was added dropwise to the calcium nitrate tetrahydrate. The pH of about 11 was obtained by the addition of ammonia solution. The reaction was carried out by heating of the reactive mixture at 80 ^{o}C for 10 min. The product was aged for 24 h in the

closed, but not sealed volume, than washed by distilled water until the washing solution was neutral. The solid fraction was separated by centrifugation. The moisture of the final HA suspension was about 90%.

2.2.2. *Alg/MWCNT+Fe suspension*

0.75 g of Alg was dissolved in 50 ml of deionized water at 37 °C for 5 h and 1.5% by weight Alg suspension was formed. 0.0025 g of MWCNT+Fe in the form of a fine powder was added to the Alg suspension, while the concentration of MWCNT+Fe in Alg solution was 0.05 mg/ml. The mixture was treated with ultrasound of low power (to prevent heating) for 20 min. As a result, a homogeneous stable Alg/MWCNT+Fe suspension has been formed.

2.2.3. *HA-Alg and HA-Alg/MWCNT+Fe beads*

6.5 g of Alg/MWCNT+Fe suspension (p.2.2.2) was added to 8 g of HA suspension (p.2.2.1) and mixed with ultrasound for 10 min. Thus, in obtained mixture the final weight ratio of dry powder MWCNT+Fe for the dry powder of HA was 0.4 mg:1 g. The mixture was dripped into a solution of 0.25 M calcium chloride for 2 h, after which the beads formed were separated from the solution by filtration, thoroughly washed with deionized water and dried at room temperature. Subsequently, the samples were called as HA-Alg/MWCNT+Fe.

For the comparison of physical and chemical properties, beads were obtained for the above technology, but without the content of MWCNT+Fe. Subsequently, these samples were called as HA-Alg (37). For further research, part of this sample was sintered at 700 °C for 1 h and the samples were called as HA-Alg (700).

2.3. Analytical Methods

2.3.1. *SEM analysis*

The surface morphology of the samples was examined using a scanning electron microscope (SEM, REMMA-102), produced by SELMI (Ukraine). Images were made in the secondary electron mode with an accelerating voltage 20 kV and a beam current of 1-10 A.

2.3.2. *XRD analysis*

The X-ray diffraction studies of the prepared samples were performed using the Shimadzu XRD-6000 diffractometer with Cu-Kα radiation. The data were collected over the 2θ range 5.0–60.0° with step of 0.02 ° and counting time of 2 s.

Identification of the crystal phases was performed using the JCPDS (Joint Committee on Powder Diffraction Standards) card catalog. More details in [48].

The average crystallite size (L; in nm) along [002] direction can be estimated from the corresponding peak broadening by the Scherrer equation

$$L = k\lambda/\beta_m \cos\theta,$$

where k is the constant, dependent on the crystallite shape (k=1 is taken), λ (in nm) is the wavelength of X-ray radiation, β_m is an integral width of (002) peak, in which physical broadening occurs only due to the small sizes of the CSR (coherent scattering region), θ is the diffraction angle.

2.3.3. *FTIR analysis*

Fourier transform infrared spectra (FTIR) were obtained using PerkinElmer Spectrum BX spectrometer in the range 400-4000 cm^{-1} (at 1 cm^{-1} resolution) for the samples pressed into the pellets of KBr.

2.3.4. *Determination of Ca/P molar ratio*

The Ca/P ratio was determined using the energy-dispersive X-ray fluorescence spectrometer ElvaX Light SDD. The spectrometer is designed for express qualitative and quantitative analysis of the composition of metal alloys, powders, liquids, deposits on the filter elements, biological samples, food products on the content of chemical elements from Na (atomic number Z=11) to U (Z=92) in a wide range of concentrations. The estimation accuracy of the mass fractions of metals in a light matrix is not worse than 1 ppm. The following parameters were used to estimate the Ca/P ratio. The voltage of the Rh anode X-ray tube was 12 kV. Calcium and phosphorous concentrations were estimated by the regression analysis method for HA samples only.

2.3.5. *TGA/DTA analysis*

The weight loss and thermal behaviour of prepared samples were investigated using Shimadzu simultaneous TGA/DTA (thermogravimetric and differential thermal analysis) analyzer DTG-60H. The samples were heated in a platinum crucible in air with the rate 10°C/min from the room temperature to 600 °C. α-Al_2O_3 was used as a standard sample.

2.3.6. *Swelling studies*

The swelling behaviour was quantified by measuring the changes in sample weight as a function of sample immersion time in phosphate buffered saline (PBS) [49] at pH=7.4. It is a water-based salt solution containing disodium hydrogen phosphate (10 mmol/l), sodium chloride (137 mmol/l), potassium chloride (2.7 mmol/l) and potassium dihydrogen phosphate (1.8 mmol/l). The osmolarity and ion concentrations of the solutions match those of the human saline. The appropriate quantity of each component was dissolved in 1 liter of distilled water to obtain the specified concentration.

The samples were in beads form and each sample mass was 0.1 g. The swollen samples were weighed after blotting with a filter paper to remove the surface liquid. The swelling ratio (S_w) was calculated using the following equation [50]

$$S_w = \frac{(W_t - W_o)}{W_o} \times 100\% ,$$

where W_0 is the initial sample weight, and W_t is the final weight of the swollen sample.

2.3.7. *Determination of drug release kinetics*

The material composition influence on the drug release was investigated in this experiment. The pharmaceutical 0.05 mas.% CH solution was used as a model drug. The beads of HA-Alg (0.17 g) and HA-Alg/MWCNT+Fe (0.17 g) were placed into 150 ml of PBS (pH=7,4) and incubated at 37 °C with continues shaking 115 rpm. The rate of drug release from composites was determined by taking of 1500 µl aliquots of PBS from each experimental tube after 1, 2, 24, 48, 72 and 120 h. An equal volume of the fresh medium then was added back to maintain a constant initial volume in the tubes. The drug release from experimental samples was studied using high-performance liquid chromatography (HPLC, Angilent Technologies 1200, detector with UV-Vis Abs, detection at λ=280 nm, column C18 (Zorbax SB-C18 4.6×150 mm, 5 µm). The data acquisition and processing was made with software Empower 2. The next mobile phase was used: 68% of 0.05 M potassium hydrogen phosphate buffer with 0.2% triethylamine (pH=3.1 at 21 ^{o}C); 32% of acetonitrile. Isostatic treatment was applied at a rate of eluent elution 2 ml/min and temperature of analytical column 40 ^{o}C. The method of eluent components pre-mixing followed by 30 min sonication was applied to reduce errors in measuring of the substance with small component concentrations.

2.3.8. *Bioactivity measurement*

Bioactivity test was carried out by soaking the samples in PBS. 0.2 mg of each sample was immersed into glass tube with 10 ml of PBS solution for 72 h. The samples were shaken at 60 rpm at 37 ^{o}C. The pH values of the PBS solution with experimental samples were measured in pre-determined time intervals using a pH meter (pH 150 MI). The pH of pure PBS (without a test samples) was taken as a control.

2.3.9. *The measurements of compressive strength*

To measure the strength under the uniaxial compression, the specimens of HA-Alg and HA-Alg/MWCNT+Fe were prepared in the form of tablets with diameter 5 mm and thickness 2 mm by cold pressing of granulated powder HA-Alg and HA-Alg/MWCNT+Fe in molds using the hydraulic press (at ~100 MPa). The mechanical properties of the specimens under loading were investigated using the original automated equipment [51].

3. Results and discussion

3.1. *SEM investigations*

Fig. 1 demonstrates the SEM images of the surface of HA-Alg/MWCNT+Fe and HA-Alg samples. The resulting images show a variety of surface structures. Thus, a more dense and homogeneous surface structure have HA-Alg/MWCNT + Fe samples compared to HA-Alg.

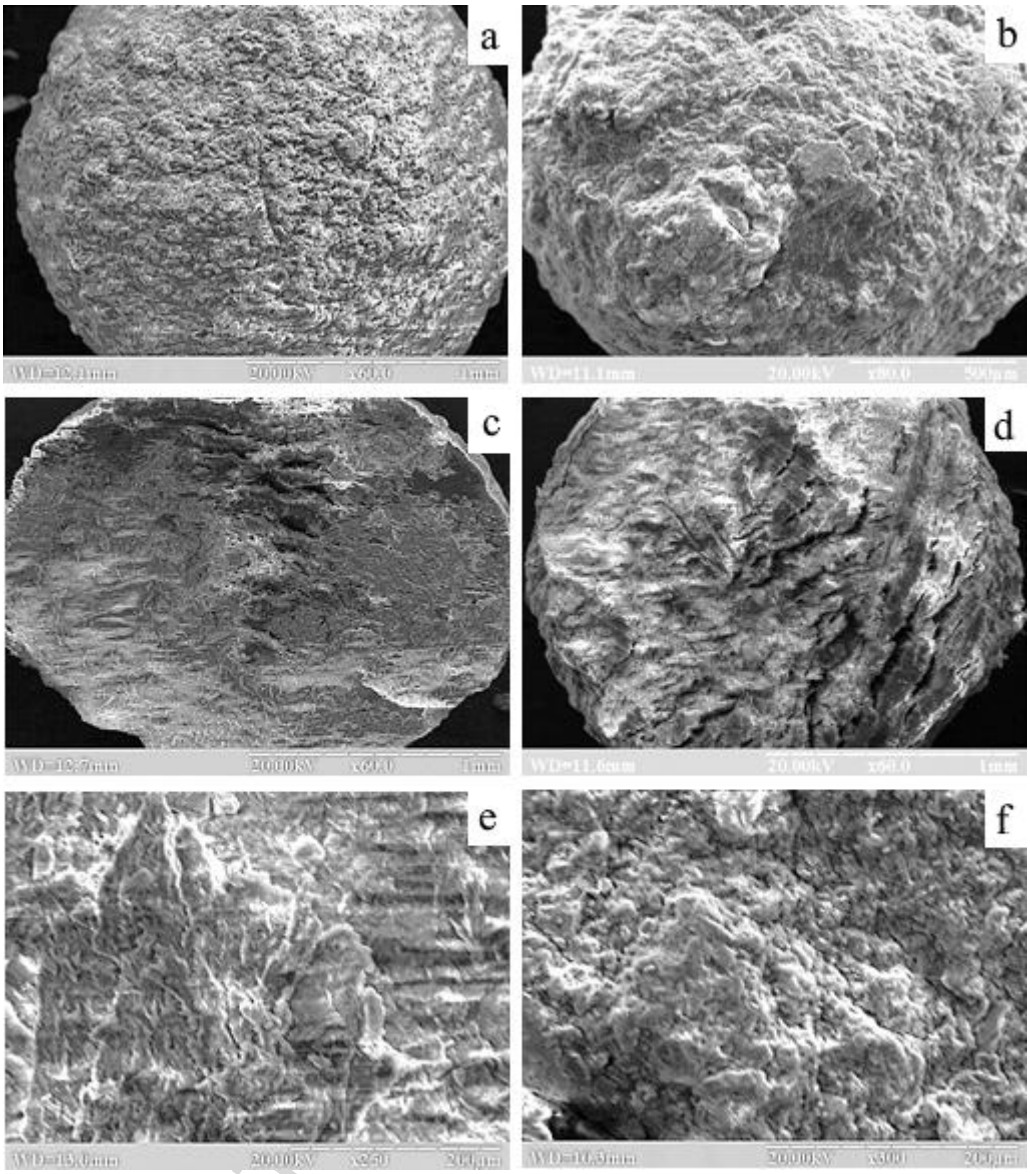

Fig. 1. SEM images: the bead surface of HA-Alg/MWCNT+Fe (a) and HA-Alg (b) samples; the cross-section of the bead of HA-Alg/MWCNT+Fe (c) and HA-Alg (d) samples; the cross section site of HA-Alg/MWCNT+Fe (e) and HA-Alg (f) samples.

3.2. *XRD investigations*

XRD investigations were carried out for the samples HA-Alg and HA-Alg/MWCNT+Fe. By the formation of the composite material, the suspension of Alg/MWCNT+Fe was added to the pre-synthesized HA, which means that it did not affect the formation of crystallites and the structure of the HA. Therefore, XRD spectra for a sample of HA-Alg dried at the temperature of 37 ^{o}C, Fig. 2(1) and sintered at 700 °C, Fig. 2(2) are shown. According to XRD, the sample of HA-Alg

contains nanoscale particles, as evidenced by the extension of reflexes for this sample. After its sintering at 700 °C, formation of monophase phosphate of apatite type and increase of its crystallinity degree was noted. Thus, the formation of the Calcium Deficiency Hydroxyapatite (PDF Number: 000-86-1201) was established.

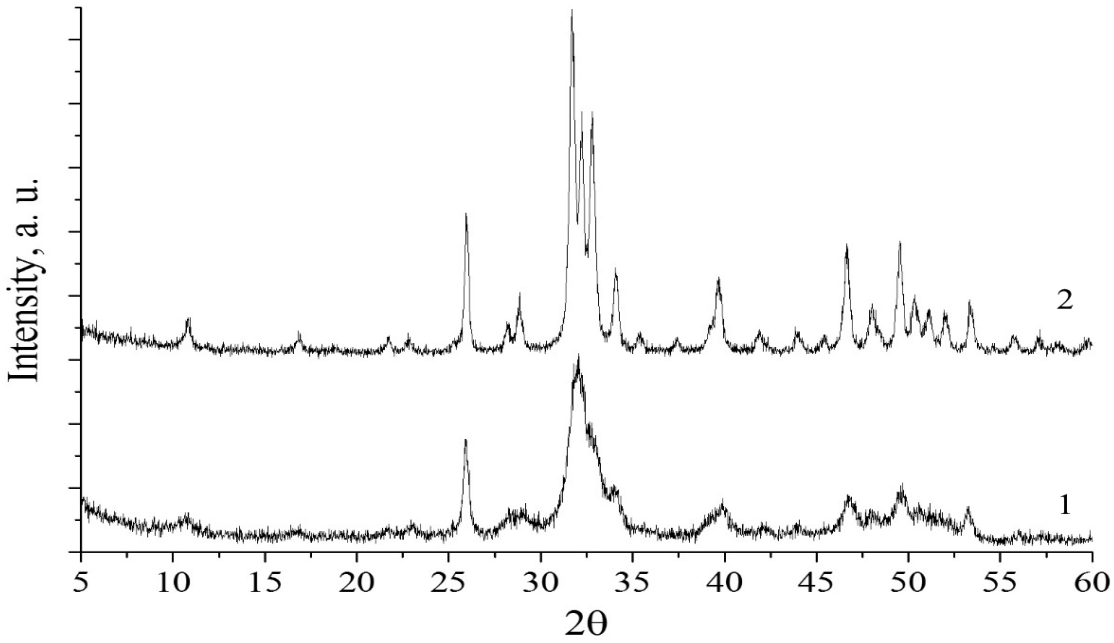

Fig. 2. Diffraction patterns from samples HA-Alg: dried at 37 °C (1) and sintered at 700 °C (2).

Table 1. Crystal structure parameters of HA-Alg samples, dried at 37 °C and sintered at 700 °C.

Sample	$L_{Scherrer}$, nm							L_{CSR}, nm	ε, 10^{-3}	a, nm	c, nm
	(002)	(211)	(112)	(300)	(202)	(401)	(213)				
37 °C	25.5	–	–	–	–	–	–	23.0	1.839	0.9354	0.6881
700 °C	37.4	28.7	25.9	26.3	37.4	29.7	35.2	33.8	0.497	0.9373	0.6865

The calculation of an *a* and *c* cell parameters showed their significantly lower values (Table 1) compared with the corresponding ones for the stoichiometric hydroxyapatite (*a*=0.9421 nm; *c*=0.6881 nm). It could be assumed that carbonate ions from reactive solution were adsorbed by HA surface during synthesis process. The further RFA analysis showed that calcium deficient carbonate-containing hydroxyapatite (Ca/P=1.52) was obtained. FTIR studies confirmed this result. It is known from literature sources [52] that B-type carbonate apatite is characterized by the decrease of the lattice parameter *a*. In addition, there are direct evidences that calcium deficient HA contains HPO_4^{2-} ions and is scarce on OH^- ions. The previous fact is confirmed by the FTIR spectra of the samples, where the librational mode of OH^- groups in HA at 630 cm^{-1} is not intensive and is overlapped by other vibrations. The value of microstrains (ε) is higher in the sample, dried at 37 ^oC due to the presence of an organic component.

3.3. *FTIR investigations*

The characteristic infrared bands of the experimental samples are shown in Fig. 3. For the comparison are given the additional data on the vibrations in pure HA and Alg (Table 2).

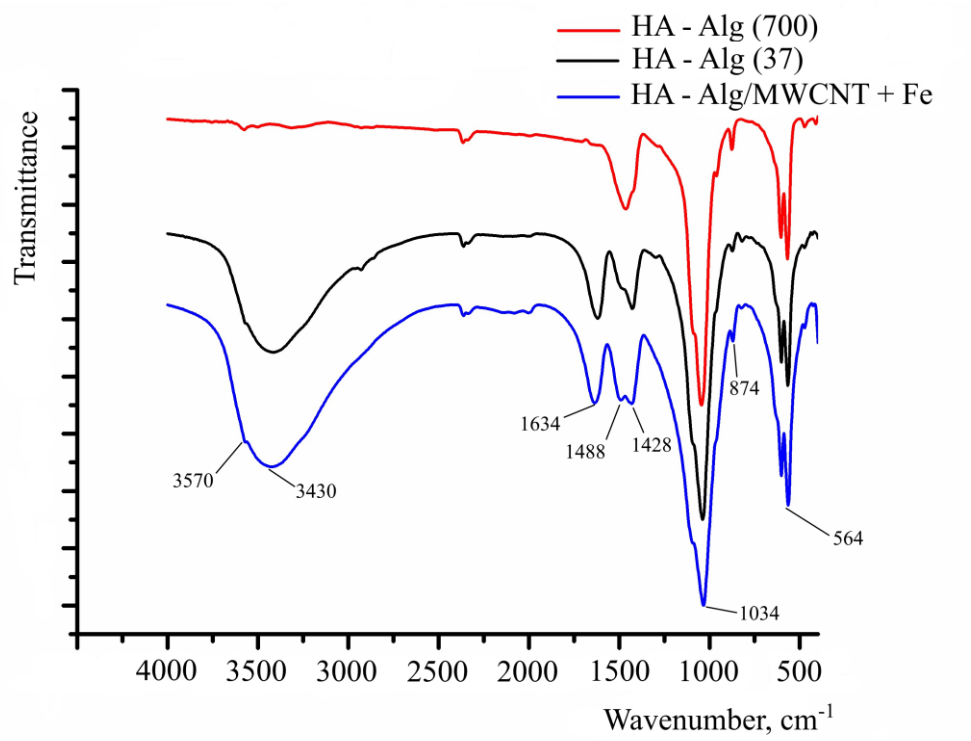

Fig. 3. FTIR spectra for investigated samples.

Table 2. Characteristic IR bands of investigated samples.

Sample/vibrational frequency (cm^{-1})					Assignments
HA-Alg (37)	HA-Alg (700)	HA-Alg/ MWCNT +Fe	Alg	HA	
476	472	472			ν_2 O-P-O in PO_4
564	570	564	572	564	ν_4 PO_4
600	602	604		602	ν_4 PO_4
-	-	-		630(week)	OH librational mode
872	876	874			ν_2 CO_3^{2-}
960	958	-		962	ν_1 P-OinPO$_4$
1038	1042	1034		1044	ν_3 P-O in PO_4
1090	1092	1096		1092	ν_3 PO_4

1430	-	1428	1422	-	COO stretch sym.
-	-	1488		-	C=C stretch
1614	-	1634	1626		ν_2 H-O-H;–C=O
2340	2334	2336			ν_2 CO_2
3416	-	3430	2924		OH stretch
3570	3576	3570	3438	3428	OH stretch

The FTIR spectra of the samples are presented in Fig. 3. In the spectra of HA-Alg(37) the hydroxyl stretching band of HA appeared at 3570 cm^{-1}, and the adsorbed water led to the broad bands centered at 1614 and 3416 cm^{-1} [53, 54]. The double peaks at 564 and 600 cm^{-1} were caused by the O–P–O bending mode (ν_4) of the phosphate group. The peak at 960 cm^{-1} corresponded to the P–O symmetric stretching mode (ν_1) of this group. The peaks at 1038 and 1090 cm^{-1} should be attributed to the asymmetric stretching mode (ν_3) of the P–O bond [55]. The weak bands at 872 cm^{-1} and 1430 cm^{-1} can be ascribed to carbonate groups, which substituted the PO_4^{3-} groups in Ca-deficient HA [56]**.** The characteristic peaks of Alg appeared at 3438, 1626 and 1422 cm^{-1}, corresponding to hydroxyl (OH), carbonyl (C=O) and carboxyl (COOH), respectively [57,58]. These bands are combined with the vibration bands of HA in the HA-Alg (37) spectra. In the FTIR spectra of HA-Alg (700) after the sintering there are no peaks associated with adsorbed water molecules (1614 and 3416 cm^{-1}). In the HA-Alg/MWCNT+Fe spectra adsorption band at 1428 cm^{-1}, corresponding to the symmetric stretching vibration of the COO^- groups, is shifted compared to HA-Alg (37) and Alg (1430 and 1422 cm^{-1}, respectively). The peak at 2928 cm^{-1} in HA-Alg (37), that is attributed to stretching vibrations of the hydrogen bonded OH^- groups in carbon acids [58], is disappeared in HA-Alg/MWCNT+Fe spectra. A band at 1488 cm^{-1} was observed for MWCNT+Fe, which can be assigned to the C=C stretching mode of the CNT network [17]. It can be assumed that carboxyl groups of the Alg molecules are ionized to COO^- ions and form bonding during HA-Alg/MWCNT+Fe composite formation.

3.4. *TGA/DTA investigation*

In studying the thermal behavior of the sample when heated to 600 °C, two areas of mass loss were noted: in the temperature range up to 100 °C (removal of water, the presence of which is confirmed by the data of FTIR spectroscopy) and in the range 200-400 °C (about 10%, removal of the organic component) (Fig. 4). It is in a good agreement with the literature data [59,60] stating that adsorbed water is gone after heating at a temperature range from 25 to 120 ^{o}C; structural water – between 120 and 300 ^{o}C; the loss of carbonate and organic components begins at 550 ^{o}C.

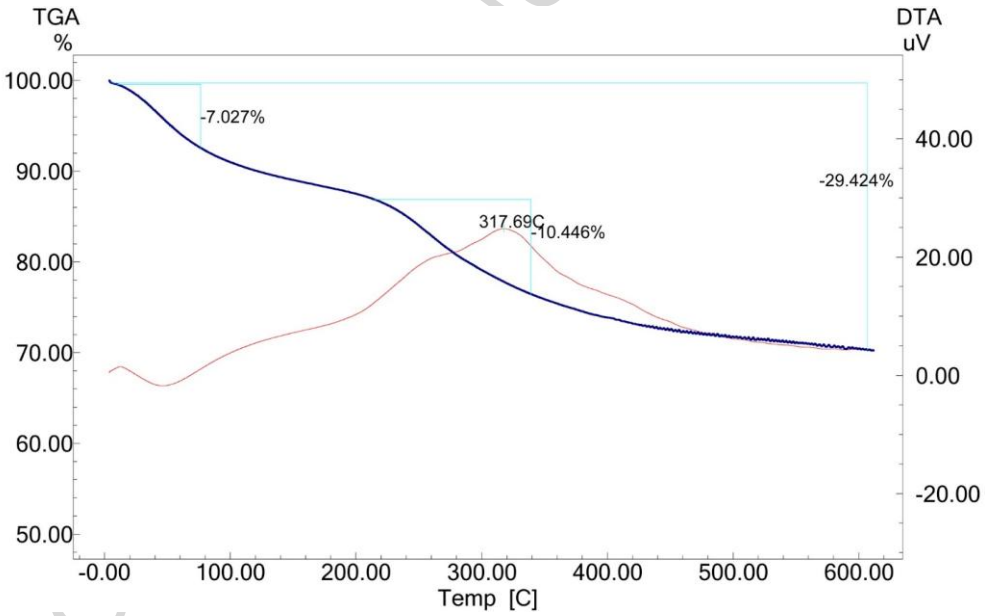

Fig. 4. TGA/DTA of the HA-Alg sample.

3.5. *Swelling studies*

In order to investigate the shape stability of the experimental samples and their ability to absorb the drug, the swelling ratio of the experimental samples in PBS was determined. The data presented in Table 3.

Table 3. Swelling ratio of the investigated samples.

Sample	Swelling, % and time of imertion	
	1 h	3 h
HA-Alg	54	68
HA-Alg/MWCNT+Fe	58	90

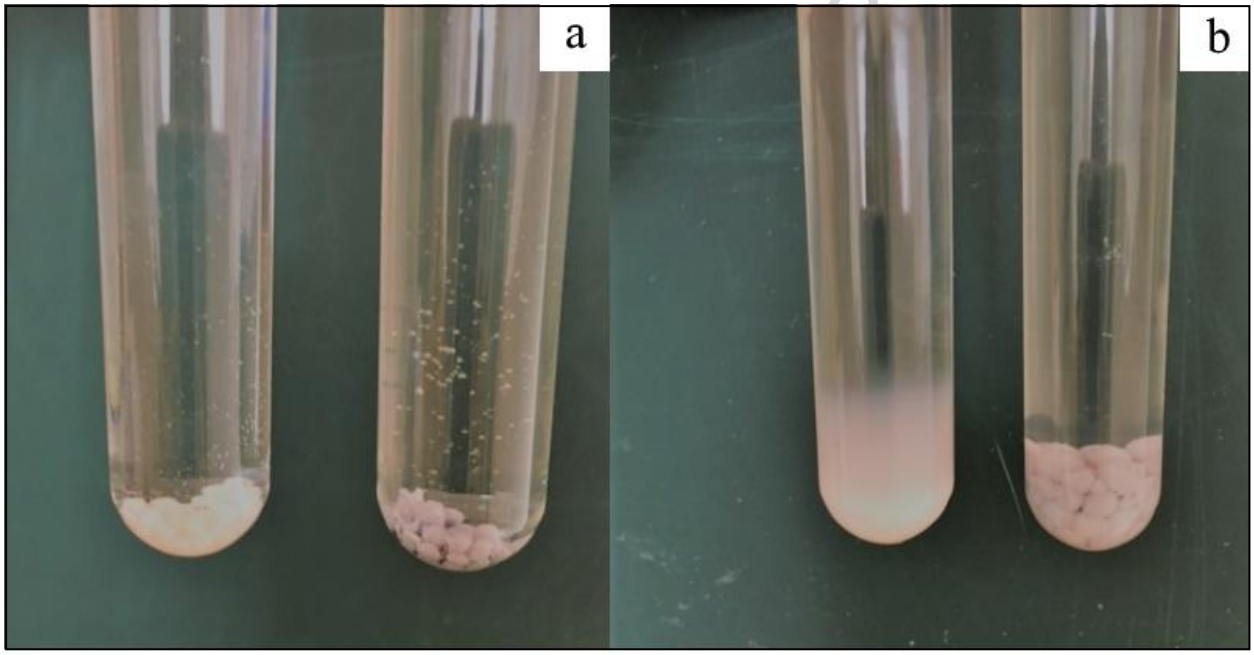

Fig. 5. Appearance of samples HA-Alg (the left tubes) and HA-Alg/MWCNT+Fe (the right tubes): immediately after being placed in PBS (a); after 7 days shaking in PBS at 37 ^{o}C (b).

Despite the fact that the results of the experiment showed a higher degree of swelling of samples with carbon tube contents, they showed greater shape stability under the influence of mechanical vibrations compared to HA-Alg (Fig. 5). The HA-Alg/MWCNT+Fe beads retained shape stability even after 7 days of shaking. At the same time, NA-Alg beads after 2 days of stay under the specified technological conditions began to lose their shape and after 7 days they became the form of colloidal solution (Fig. 5,b). These results can be explained by the fact that when the MWCNT+Fe powder is introduced into composite material by the synthesis, the polyelectrolyte reactions between Alg, HA and MWCNT+Fe take place. In this case the

enhancing of cross-linking rate provides more stable beads form. So, the ability of HA-Alg beads to maintain their structural integrity is enhanced with MWCNT+Fe addition.

3.6. *Bioactivity studies*

Bioactivity tests were carried out by soaking the samples in PBS with pH=7.47. The glass tubes with 0.2 mg of each sample beads shaked in 10 ml of PBS with 60 rpm at 37 ^{0}C. The pH values measured after a certain time intervals and results presented in Fig. 6. The pure PBS was used as a control.

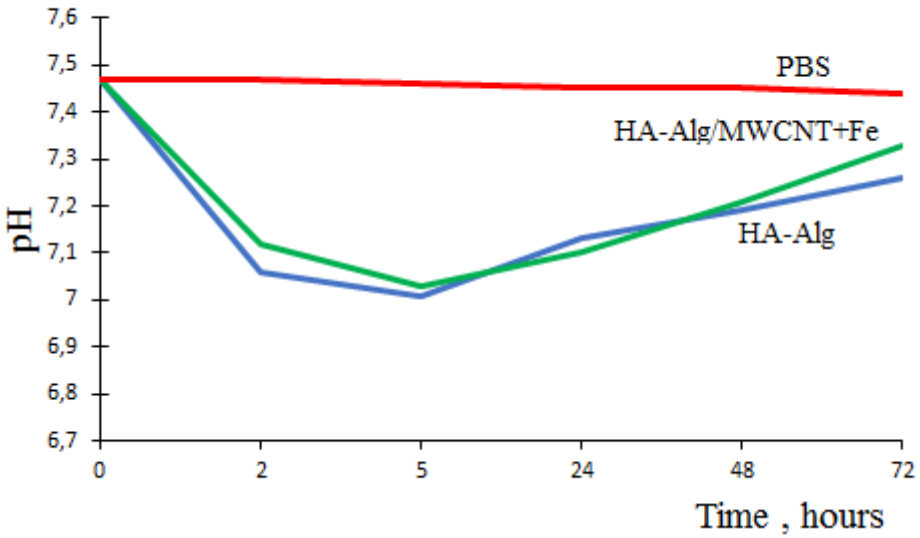

Fig. 6. Changes of pH values in PBS due to the immersion of the samples.

Bioactivity test showed, that pH of the control PBS (without experimental samples) remained constant during the experiment (Fig. 6). At the same time, the pH values of PBS with immersed samples varied throughout the experiment, that indicates their bioactivity, which depends on the crystallite sizes, grain sizes, shape and defectiveness. A decrease of the pH

values for HA-Alg and HA-Alg/MWCNT+Fe samples during the first 5 h could be due to the presence of amorphous calcium phosphate phase (ACP) and its transformation into the stable HA phase causing the release of acidic ion of HPO_4^{2-} [61]. The increase of pH values after 5 h is due to the partial dissolution on the sample surfaces and indicates the high reactivity of these materials. These facts are in agreement with the formation mechanisms of the new apatite layer on the bioactive surface –an exchange occurs between Ca^{2+} and H^+ or H_3O^+ from the solution. Such exchanges provoke an increase of the pH that favors the formation of apatite nuclei [62]. The gradual increase of the pH values could also be due to the presence of carbonate impurities [63]. In this context it is important to note that MWCNT as well as MWCNT+Fe nanoparticles do not manifest any toxic effect *in vitro* at the concentrations used in our experiment [64,65].

3.7. *HPLC study*

For HPLC studies were prepared the samples containing CH, as a reference drug. The CH is active against gram-positive and gram-negative organisms, facultative anaerobes, aerobes, and yeasts [66]. It is used in disinfectants (disinfection of the skin and hands), cosmetics (additive to creams, toothpaste, deodorants, and antiperspirants), and pharmaceutical products (preservative in eye drops, active substance in wound dressings and antiseptic mouthwashes [67]. The CH was introduced into composites by the method of saturation. For this, 0.2 g of each sample (HA-Alg and HA-Alg/MWCNT+Fe) was immersed in 4 ml of CH solution for 60 min with following drying at 37 ^oC. In order to evaluate the CH release kinetics, the each drug contained sample was placed to the tube with 15 ml of PBS. The tubes with samples were shaked (rpm 115, temperature 37 ^oC) for 120 h. The quantity of released CH was plotted against the incubation time (Fig. 7).

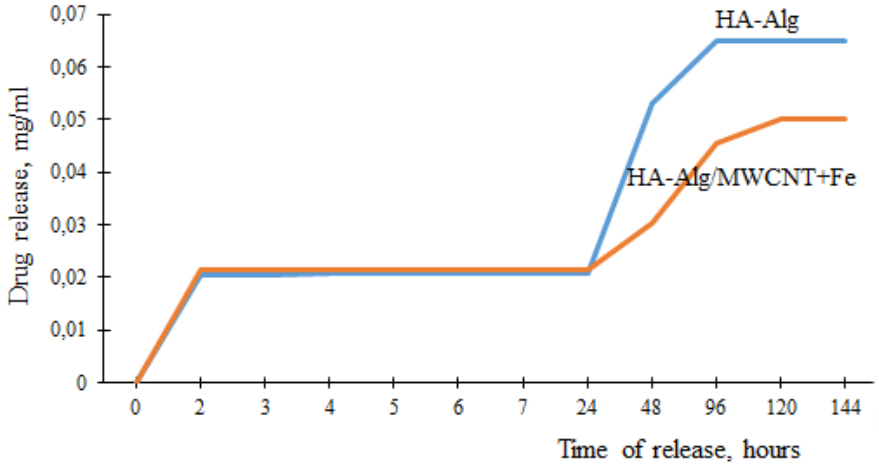

Fig. 7. CH release kinetic from the HA-Alg and HA-Alg/MWCNT+Fe beads.

In the Fig. 7 we observe 3 main stages of the CH release: for the first 2 h, within 24 h, after 24 h. The driving force of the process is the concentration gradient CH in the system "composite (maximum concentration) - PBS (zero concentration)". Studies have shown that during the first 2 h, the release of the drug from both samples occurs with practically the same speed. It is evident that the first stage of drug release is due to surface molecules of CH, which have less binding energy to the composite surface. The second stage of the drug release is the result of a slow exchange of CH molecules with water molecules of the PBS due to swelling of the sample. The third intensive release stage after 24 h of shaking in PBS is due to the partial destruction of the composite shape and structure, as a result of maximum hydration, that led to increase of drug diffusion ability. A full release of the drug, absorbed by HA-Alg sample, took place for 96 h of shaking in PBS. The CH release from HA-Alg/MWCNT+Fe lasted for 120 h. The release rate from the HA-Alg sample is higher compared to HA-Alg/MWCNT+Fe one. The presence of MWCNT+Fe significantly inhibits this process and the drug release time from HA-Alg/MWCNT+Fe is prolonged. It is obviously connected with the features of the interaction

mechanism of the surface MWCNT+Fe with CH. The ability of HA-Alg to maintain its structural integrity and shape stability is enhanced with MWCNT+Fe addition (Fig. 5).

3.8. *Compressive strength studies*

The results of the studies of compressive strength of different types of HA-based composites are presented in Table 4 and Fig. 8.

Table 4. Strength properties of HA-based composites.

Specimen	Density, g/cm^3	Maximal relative deformation, ε_{destr}	Strength σ_c, MPa	Young's modulus E, MPa
HA-Alg	2.21	0.25	118	570
HA-Alg/MWCNT+Fe	2.27	0.23	168	740

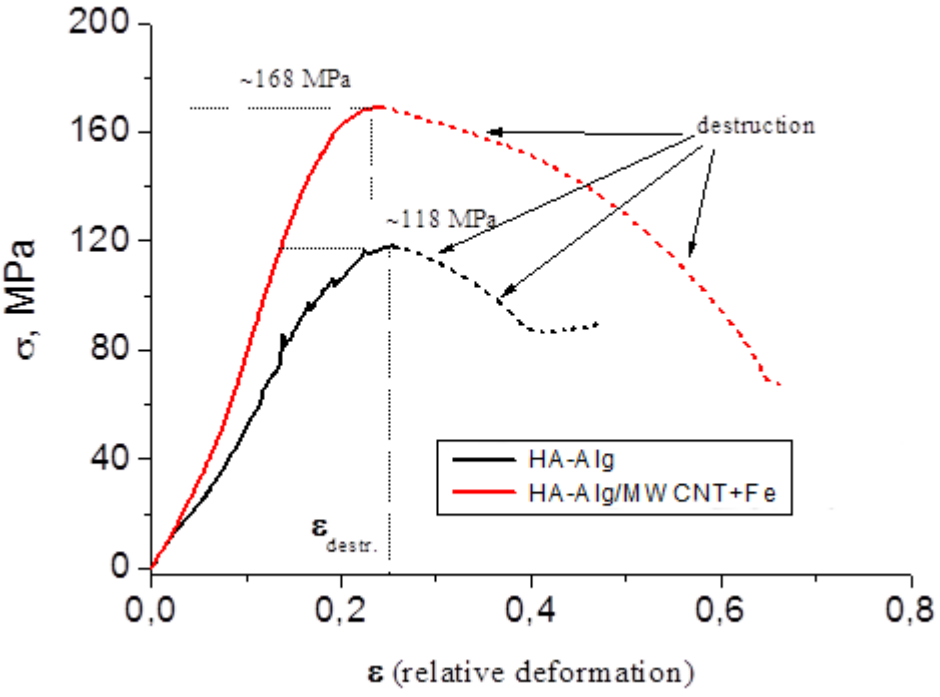

Fig. 8. Strength σ_c of the HA-Alg and HA-Alg/MWCNT+Fe beads measured at uniaxial compression.

As one can seen from Fig. 8, the addition of MWCNT+Fe into HA-Alg increases the compressive strength of specimen. The maximal relative deformations ε_{destr} before destruction are approximately equal to ~0.23-0.25 for two types of specimens. In general, such increase of strength for HA-Alg-MWCNT+Fe sample is related to high aspect ratio and excellent mechanical properties of MWCNT. On the other hand, it is known [68], that the interfacial adhesion between the composite components determines the load, which will be transferred between them. Thus, the increase of the strength for HA-Alg/MWCNT+Fe may be also explained by well bonding of MWCNT+Fe nanoparticles to the HA-Alg matrix, that leads to efficient stress transfer at the MWCNT+Fe.

Finally, the Young's modulus (E) estimation for three compression-unloading cycles of the samples has shown that they had a fairly high Young's modulus, namely E~570 MPa for HA-Alg and E~740 MPa for HA-Alg/MWCNT+Fe, that is comparable to a steel sample of the same size (E~706 MPa).

Thus, a composite material HA-Alg/MWCNT+Fe in the form of beads was created and studied. Each ingredient of a composite performs its main function: HA provides osteoconductivity and biocompatibility; Alg promotes homogenization of the composite material, increases biocompatibility, gives the material plasticity, makes it possible to form the beads; MWCNTs+Fe enhances mechanical properties, affect the dynamics of drug release. The ability of Alg to gelation provides the creation of a biopolymer matrix with the immobilized particles of the inorganic component (HA, MWCNT+Fe). The mixing Alg with MWCNT+Fe powder, followed by ultrasound processing during synthesis leads to the formation of a homogeneous colloidal solution. Alg promotes to the uniform distribution of MWCNT+Fe particles, since the carboxylic groups of the biopolymer form complexes with iron ions, which is proved by the FTIR results. The cross-linking of Alg molecules with calcium ions at the last

stage of synthesis leads to the formation of biopolymer apatite beads. This form of material provides filling of bone defects of complex geometry with a minimum gap between the bone and the implant. The spaces between the beads will act as a macropore and will contribute to the formation of new bone tissue throughout the volume of the implant.

Conclusions

Thus, the novel polymer-apatite composite material containing MWCNT+Fe nanoparticles was synthesized by the method of "wet chemistry". The interaction between organic and inorganic components in the composite material has been proved by FTIR spectroscopy. When the MWCNT+Fe powder is introduced into composite material the polyelectrolyte reaction between Alg, HA and MWCNT+Fe takes place. The ability of HA-Alg beads to maintain its structural integrity is enhanced with MWCNT+Fe addition. The drug release from HA-Alg/MWCNT+Fe continued 24 h longer, compared to HA-Alg, that connected with the features of the interaction mechanism of the surface MWCNT+Fe with CH. The increase of the strength for HA-Alg/MWCNT+Fe takes place and can be also explained by well bonding of MWCNT+Fe nanoparticles to the HA-Alg matrix, that leads to efficient stress transfer at the MWCNT+Fe. Finally, HA-Alg/MWCNT+Fe sample is characterized by a high Young's modulus comparable to steel.

Hence, this novel composite material opens the possibility of its use in bioengineering of bone tissue to fill bone defects of various geometries with the function of prolonged release of the drug. Potentially the material can be used in 3D modeling of areas of bone tissue that have to bear a mechanical load.

References

1 S.V. Dorozhkin, Amorphous calcium orthophosphates: nature, chemistry and biomedical applications, Int. J. Mater. Chem. 2 (2012) 19-46.

2 W. Bojar, M. Kucharska, T. Ciach, Ł. Koperski, Z. Jastrzębski, M. Szałwiński, Bone regeneration potential of the new chitosan-based alloplastic biomaterial, J. Biomater. Appl. 28 (2014) 1060-1068.

3 N.S. Pawar, K.J. Edgar, Alginate derivatization: A review of chemistry, properties and applications, Biomaterials 33 (2012) 3279-3305.

4 I. Liakos, L. Rizzello, I.S. Bayer, P.P. Pompa, R. Cingolani, A. Athanassiou, Controlled antiseptic release by alginate polymer films and beads, Carbohydrate Polymers 92 (2013) 176–183.

5 L.F. Sukhodub, L.B. Sukhodub, In. Chorna, Chitosan-apatite composites: synthesis and properties, Biopolym. Cell 32 (2016) 83–97.

6 A. Banerjee, D. Nayak, S. Lahiri, A new method of synthesis of iron doped calcium alginate beads and determination of iron content by radiometric method, Biochem. Eng. J. 33 (2007) 260–262.

7 M. George, T.E. Abraham, PH sensitive alginate–guar gum hydrogel for the controlled delivery of protein drugs, Int. J. Pharm. 335 (2007) 123–129.

8 Q. Wang, X. Hu, Y. Du, J.F. Kennedy, Alginate/starch blend fibers and their properties for drug controlled release, Carbohydrate Polymers 82 (2010) 842–847.

9 C.H. Goh, P.W.S. Heng, L.W. Chan, Alginates as a useful natural polymer for microencapsulation and therapeutic applications, Carbohydrate Polymers 88 (2012) 1–12.

10 D.C. Manatunga, R.M. de Silva, K.M.N. de Silva, N. de Silva, S. Bhandari, Y.K. Yap, N.P. Costha, pH responsive controlled release of anti-cancer hydrophobic drugs from sodium alginate and hydroxyapatite bi-coated iron oxide nanoparticles, Eur. J. Pharm. Biopharm. 117 (2017) 29-38.

11 A. Kovtun, D. Kozlova, K. Ganesan, C. Biewald, N. Seipold, P. Gaengler, W.H. Arnold, M. Epple, Chlorhexidine-loaded calcium phosphate nanoparticles for dental maintenance treatment: combination of mineralising and antibacterial effects, RSC Adv. 2 (2012) 870–875.

12 P. Turon, L.J. del Valle, C. Alemán, J. Puiggali, Biodegradable and biocompatible systems based on hydroxyapatite nanoparticles, Appl. Sci. 7 (2017) 60.

13 S. Nahorny, H. Zanin, V.A. Christino, F.R. Marciano, A.O. Lobo, L.E.S. Soares, Multi-walled carbon nanotubes/graphene oxide hybrid and nanohydroxyapatite composite: A novel coating to prevent dentin erosion, Mater. Sci. Eng. C 79 (2017) 199-208.

14 S. Iijima, Helical microtubules of graphite carbon, Nature, 354 (1991) 56-58.

15 A.A. White, S.M. Best, I.A. Kinloch, Hydroxyapatite–carbon nanotube composites for biomedical applications: A review, Int. J. Appl. Ceram. Technol., 4 (2007) 1–13.

16 M. Kawaguchi, T. Fukushima, T. Hayakawa, N. Nakashima, Y. Inour, S. Takeda, K. Okamura, K. Taniguchi, Preparation of carbon-alginate nanocomposite gel for tissue engineering, Dental Mater J. 25 (2006) 719-725.

17 A.S. Khan, A.N. Hussain, L. Sidra, Z. Sarfraz, H. Khalid, M. Khan, F. Manzoor, L. Shahzadi, M. Yar, I.U. Rehman, Fabrication and *in vivo* evaluation of hydroxyapatite/carbon nanotube electrospun fibers for biomedical/dental application, Mater. Sci. Eng. C 80 (2017) 387-396.

18 R. Chakraborty, V.S. Seesala, M. Sen, S. Sengupta, S. Dhara, P. Saha, K. Das, S. Das, MWCNT reinforced bone like calcium phosphate—hydroxyapatite composite coating developed through pulse, cytocompatibility and corrosion protection performance compared to bare metallic implant surface, Surf. Coatings Technol. 325 (2017) 496–514.

19 R. Rajesh, N. Senthilkumar, A. Hariharasubramanian, Y. Dominic Ravichandran, Review on hydroxyapatite-carbon nanotube composites and some of their applications, Int. J. Pharm. Pharm. Sci. 4 (2012) 23-27.

20 S.K. Srivastava, V.K. Gupta, S. Jain, Determination of lead using a poly(vinyl-chloride)-based crown ether membrane, Analyst 120 (1995) 495–498.

21 S.K. Srivastava, V.K. Gupta, M.K. Dwivedi, S. Jain, Caesium PVC-Crown (Dibenzo-24-crown-8) based membrane sensor, Anal. Proceedings Including Anal. Commun. 32 (1995) 21–23.

22 S.K. Srivastava, V.K. Gupta, S. Jain, PVC-based 2,2,2-Cryptand sensor for zinc ions, Anal. Chem. 68 (1996) 1272-1275.

23 V.K. Gupta, A. Nayak, S. Agarwal, B. Singhal, Recent advances on potentiometric membrane sensors for pharmaceutical analysis, Combinatorial Chem. High Throughput Screen., 14 (2011) 284-302.

24 V.K. Gupta, M.R. Ganjali, P. Norouzi, H. Khani, A. Nayak, S. Agarwal, Electrochemical analysis of some toxic metals by ion–selective electrodes, Crit. Rev. Anal. Chem. 41 (2011) 282-313.

25 V.K. Gupta, L.P. Singh, R. Singh, N. Upadhyay, S.P. Kaur, B. Sethi, A novel copper (II) selective sensor based on Dimethyl 4, 4′ (o-phenylene) bis(3-thioallophanate) in PVC matrix, J. Mol. Liq. 174 (2012) 11–16.

26 S. Karthikeyan, V.K. Gupta, R. Boopathy, A. Titus, G. Sekaran, A new approach for the degradation of high concentration of aromatic amine by heterocatalytic Fenton oxidation: Kinetic and spectroscopic studies, J. Mol. Liq. 173 (2012) 153–163.

27 V.K. Gupta, B. Sethi, R.A. Sharma, S. Agarwal, A. Bharti, Mercury selective potentiometric sensor based on low rim functionalized thiacalix[4]-arene as a cationic receptor, J. Mol. Liq. 177 (2013) 114–118.

28 V.K. Gupta, A.K. Singh, L.K. Kumawat, Thiazole schiff base turn-on fluorescent chemosensor for Al^{3+} ion, Sensors Actuators B 195 (2014) 98–108.

29 M.L. Yola, V.K. Gupta, T. Eren, A.E. Sen, N. Atar, A novel electro analytical nanosensor based on graphene oxide/silvernanoparticles for simultaneous determination of quercetin and morin, Electrochimica Acta 120 (2014) 204–211.

30 V.K. Gupta, S. Kumar, R. Singh, L.P. Singh, S.K. Shoora, B. Sethi, Cadmium (II) ion sensing through p-tert-butyl calix[6]arene based potentiometric sensor, J. Mol. Liq. 195 (2014) 65–68.

31 V.K. Gupta, H. Karimi-Maleh, R. Sadegh, Simultaneous determination of hydroxylamine, phenol and sulfite in water and waste water samples using a voltammetric nanosensor, Int. J. Electrochem. Sci. 10 (2015) 303–316.

32 V.K. Gupta, N. Mergu, L.K. Kumawat, A.K. Singh, Selective naked-eye detection of Magnesium (II) ions using acoumarin-derived fluorescent probe, Sensors Actuators B 207 (2015) 216–223.

33 V.K. Gupta, N. Mergu, L.K. Kumawat, A.K. Singh, A reversible fluorescence "off-on-off" sensor for sequential detection of aluminum and acetate/fluoride ions, Talanta 144 (2015) 80-89.

34 H. Karimi-Maleh, F. Tahernejad-Javazmi, N. Atar, M.L. Yola, V.K. Gupta, A.A. Ensafi, A novel DNA biosensor based on a pencil graphite electrode modified with polypyrrole/functionalized multiwalled carbon nanotubes for determination of 6 mercaptopurine anticancer drug, Ind. Eng. Chem. Res. 54 (2015) 3634–3639.

35 M.H. Dehghani, D. Sanaei, I. Ali, A. Bhatnagar, Removal of chromium(VI) from aqueous solution using treated waste newspaper as a low-cost adsorbent: Kinetic modeling and isotherm studies, J. Mol. Liq. 215 (2016) 671–679.

36 H. He, L.A. Pham-Huy, P. Dramou, D. Xiao, P. Zuo, C. Pham-Huy, Carbon nanotubes: Applications in pharmacy and medicine, BioMed. Res. Int. (2013) 578290.

37 S. Kumar, R. Rani, N. Dilbaghi, K. Tankeshwar, K.-H. Kim, Carbon nanotubes: a novel material for multifaceted applications in human healthcare, Chem. Soc. Rev. 46 (2017) 158-196.

38 S. Prylutska, R. Bilyy, T. Shkandina, D. Rotko, A. Bychko, V. Cherepanov, R. Stoika, V. Rybalchenko, Yu. Prylutskyy, N. Tsierkezos, U. Ritter, Comparative study of membranotropic action of single- and multi-walled carbon nanotubes, J. Biosci. Bioeng. 115 (2013) 674-679.

39 O.P. Matyshevska, A.Yu. Karlash, Ya.V. Shtogun, A. Benilov, Yu. Kirgizov, K.O. Gorchinskyy, E.V. Buzaneva, Yu.I. Prylutskyy, P. Scharff, Self-organizing DNA/carbon nanotube molecular films, Mater. Sci. Eng. C 15 (2001) 249-252.

40 S. Marchesan, M. Melchionna, M. Prato, Carbon nanostructures for nanomedicine: Opportunities and challenges. Fullerenes, Nanotubes, Carbon Nanostruct. 22 (2014) 190-195.

41 A. Burlaka, S. Lukin, S. Prylutska, O. Remeniak, Yu. Prylutskyy, M. Shuba, S. Maksimenko, U. Ritter, P. Scharff, Hyperthermic effect of multi-walled carbon nanotubes stimulated with near infrared irradiation for anticancer therapy: *in vitro* studies, Exp. Oncol. 32 (2010) 48-50.

42 R. L. Price, M. C. Waid, K. M. Haberstroh, and T. J. Webster, Selective bone cell adhesion on formulations containing carbon nanofibers, Biomaterials 24 (2003) 1877–1887.

43 S.V. Prylutska, I.I. Grynyuk, S.M. Grebinyk, O.P. Matyshevska, Yu.I. Prylutskyy, U. Ritter, C. Siegmund, P. Scharff, Comparative study of biological action of fullerenes C_{60} and carbon nanotubes in thymus cells, Mat.-wiss. u. Werkstofftech. 40 (2009) 238-241.

44 S. Prylutska, R. Bilyy, T. Schkandina, A. Bychko, V. Cherepanov, K. Andreichenko, R. Stoika, V. Rybalchenko, Yu. Prylutskyy, P. Scharff, U. Ritter, Effect of iron-doped multi-

walled carbon nanotubes on lipid model and cellular plasma membranes, Mater. Sci. Eng. C 32 (2012) 1486-1489.

45 N. Kobayashi, H. Izumi, Y. Morimoto, Review of toxicity studies of carbon nanotubes, J. Occup. Health 59 (2017) 394-407.

46 G.E. Grechnev, V.A. Desnenko, A.V. Fedorchenko, A.S. Panfilov, L.Yu. Matzui, Yu.I. Prylutskyy, M.I. Grybova, U. Ritter, P. Scharff, Yu.A. Kolesnichenko, Structure and magnetic properties of multi-walled carbon nanotubes modified with iron, Low Temp. Phys. 36 (2010) 1086-1090.

47 A.S. Stanislavov, L.F. Sukhodub, L.B. Sukhodub, V.N. Kuznetsov, K.L. Bychkov, M.I. Kravchenko, Structural features of hydroxyapatite and carbonated apatite formed under the influence of ultrasound and microwave radiation and their effect on the bioactivity of the nanomaterials, Ultrasonics - Sonochemistry 42 (2018) 84–96.

48 V.M. Kuznetsov, L.B. Sukhodub, L.F. Sukhodub, Structural and substructural features of apatite-biopolymer composites: the comparison of data obtained using X-ray diffraction and scanning electron microscopy with electron diffraction, J. Nano-Electron. Phys. 6 (2014) 04039.

49 A.T. Palasz, P.B. Brena, The effect of different zwitterionic buffers and PBS used for out-of-incubator procedures during standard in vitro embryo production on development, morphology and gene expression of bovine embryos, Theriogenology 70 (2008) 1461-1470.

50 Y. Han, Q. Zeng, H. Li, J. Chang, The calcium silicate/alginate composite: Preparation and evaluation of its behavior as bioactive injectable hydrogels. Acta Biomater. 9 (2013) 9107-9117.

51 L. Vovchenko, O. Lazarenko, L. Matzui, Yu. Perets, A. Zhuravkov, V. Fedorets, F. Le Normand, Mechanical and electrical properties of the epoxy composites with graphite nanoplatelets and carbon nanotubes, Phys. St. Sol. A 211 (2014) 336-341.

52 J.C. Elliot, Structure and chemistry of the apatites and other calcium orthophosphates, Amsterdam-London-NewYork-Tokyo, 1994, pp.389.

53 W.F. Neuman, T.Y. Toribara, B.J. Mulryan, The surface chemistry of bone. Carbonate: Phosphate exchange, J. Am. Chem. Soc. 78 (1956) 4263-4266.

54 J. Arends, J. Christoffersen, M.R. Christoffersen, H. Eckert, B.O. Fowler, J.C. Heughebaert, G.H. Nancollas, J.P. Yesinowski, S.J. Zawacki, A calcium hydroxyapatite precipitated from an aqueous solution; an international multimethod analysis, J. Crystal Growth 84 (1987) 515-532.

55 M. Rajkumar, N. Meenakshisundaram, V. Rajendra, Development of nanocomposites based on hydroxyapatite/sodium alginate: Synthesis and characterization, Mater. Charact. 62 (2011) 469-479.

56 R. Pereira, A. Carvalho, D.C. Vaz, M.H. Gil, A. Mendes, P. Bártolo, Development of novel alginate based hydrogel films for wound healing applications, Int. J. Biol. Macromol. 52 (2013) 221-230.

57 B.O. Fowler, Infrared studies of apatites. Vibrational assigments for calcium, strontium and barium hydroxyapatites utilizing osotopic substitution. Inorg. Chem. 13 (1974) 194-207.

58 V. Kumar Malesu, D. Sahoo, P.L. Nayak, Chitosan-sodium alginate nanocomposites blended with cloisite 30b as a novel drug delivery system for anticancer drug curcumin, Int. J. Appl. Biol. Pharm. 2 (2011) 402-411.

59 J.C. Elliot, Calcium phosphate biominerals, Rev. Mineral. Geochem. 48 (2002) 426-423.

60 N. Strutynska, I. Zatovsky, N. Slobodyanik, A. Malyshenko, Y. Prylutskyy, O. Prymak, I. Vorona, S. Ishchenko, N. Baran, A. Byeda, A. Mischanchuk, Preparation, characterization, and thermal transformation of poorly crystalline sodium- and carbonate-substituted calcium phosphate, Eur. J. Inorg. Chem. (2015) 622-629.

61 A. Farzadi, M. Solati-Hashjin, F. Bakhshi, A. Aminian, Synthesis and characterization of hydroxyapatite/b-tricalcium phosphate nanocomposites using microwave irradiation, Ceram. Int. 37 (2011) 65-71.

62 A.O. Lobo, H. Zanin, I.A. Siqueira, N.C. Leite, F.R. Marciano, E.J. Corat, Effect of ultrasound irradiation on the production of nHAp/MWCNT nanocomposites, Mater. Sci. Eng. C 33 (2013) 4305-4312.

63 T.S.S. Kumar, I. Manjubala, J. Gunasekaran, Synthesis of carbonated calcium phosphate ceramics using microwave irradiation, Biomaterials 21 (2000) 1623-1629.

64 S.V. Prylutska, I.I. Grynyuk, O.P. Matyshevska, V.M. Yashchuk, Yu.I. Prylutskyy, U. Ritter, P. Scharff, Estimation of multi-walled carbon nanotubes toxicity *in vitro*, Physica E 40 **(**2008) 2565-2569.

65 M. Tolkachov, V. Sokolova, V. Korolovych, Yu. Prylutskyy, M. Epple, U. Ritter, P. Scharff, Study of biocompatibility effect of nanocarbon particles on various cell types *in vitro*, Mat.-wiss. u. Werkstofftech. 47 (2016) 216-221.

66 J.B. Leikin, F.P. Paloucek, Chlorhexidine Gluconate, Poisoning and Toxicology Handbook, 4th ed., Informa, 2008, pp. 183-184.

67 T. Güthner, B. Mertschenk, B. Schulz, Guanidine and Derivatives, Ullman's Encyclopedia of Industrial Chemistry, 7th ed., Wiley, 2007, pp. 13.

68 S. Fu, X. Feng, B. Lauke, Y. Mai, Effects of particle size, particle/matrix interface adhesion and particle loading on mechanical properties of particulate-polymer composites, Compos. B Eng. 39 (2008) 933-961.

Highlights

“Composite material based on hydroxyapatite and multi-walled carbon nanotubes filled by iron: preparation, properties and drug release ability”.

In the submitted manuscript, we have revealed for the first time that novel bioactive composite material based on hydroxyapatite and multi-walled carbon nanotubes filled by iron can be synthesized by the "wet chemistry" method. Bioactivity test was carried out by soaking the samples in PBS. The material composition influence on the model drug release was studied using HPLC methods. The findings demonstrate the possibility for a application of the created composite material in bioengineering of bone tissue to fill bone defects of various geometries with the function of prolonged release of the drug. It is assumed that this composite material can be used in 3D modeling of areas of bone tissue that have to bear a mechanical load.